Received: April 30, 2020
Revised: June 3, 2020
Accepted: June 10, 2020

Structural, morphological and photoluminescence properties of Ga- and F-doped ZnO nanorod-structured films grown by hydrothermal process on ZnO sol-gel derived seeding films

Orawan Tanomkiat[1], Amara Kiewrugsa[2], Apichart Sungthong[2] and Krisana Chongsri[2,*]

[1] *Energy Technology and Management Faculty of Science Energy and Environment, King Mongkut's University of Technology North Bangkok Rayong Campus, 21120, Thailand*

[2] *Department of Applied Physics, Faculty of Science and Technology, Rajabhat Rajanagarindra University, Chachoengsao 24000, Thailand*

Abstract

In this work, structural and morphological properties of ZnO, Ga-doped ZnO, and F-doped ZnO nanorod-structured (NRS) films grown by the hydrothermal process were extensively investigated. Undoped ZnO, 5% Ga-doped ZnO and 5% F-doped ZnO nanorod-structured films were fabricated on sol-gel derived ZnO seeding layer by one-step hydrothermal process operated at 90 ºC for 2 hours using zinc nitrate hexahydrate, gallium (III) nitrate hydrate, and ammonium fluoride as Zn, Ga and F source, respectively. The corresponding SEM results indicated that both Ga and F dopants played significant roles in morphological properties of grown nanorod structures such as preferential orientation, shape, and size. The photoluminescence (PL) spectroscopy at room temperature and low temperature was conducted in order to investigate the effect of both dopants on luminescence properties of ZnO-based NRS. The corresponding PL spectra exhibited stronger yellow-orange emission intensity of the F-doped NRS implying greater oxygen vacancy defects of ZnO lattice induced by F dopant.

Keywords: Nanorod, Ga-doped ZnO, F-doped ZnO

1. Introduction

Zinc oxide (ZnO) is an n-type semiconductor compound with a wide band gap (Eg~3.2–3.4 eV) at 300 K and relatively large exciton binding energy (60 meV). ZnO nanostructures have been extensively utilized as potential optoelectronic materials due to the combination of their exceptional electrical and optical properties. The applications of ZnO-based materials for practical devices such as light-emitting devices [1], gas sensors [2], chemical sensors [3], pressure sensors [4], solar cells [5-6], and ultraviolet detectors [7-8] have been greatly developed. Moreover, further improved electrical and optical properties of ZnO are still required for specific applications, especially for optoelectronics devices. Doping with proper elements including Al [9], In [9-10], Ga [11], Mg [12], N [13], and F [14] have been recognized as one of the effective routes for enhancing its functional properties. Among dopants, Ga as a cation and F as an anion can be considered to be potential candidates as the dopants to effectively improve relevant ZnO properties. It has been reported that Ga dopants could result in greatly improved electrical conductivity [15], a blue shift in optical band gap [16], and even specific surface area of ZnO nanostructures [17]. Meanwhile, it has been notified that F dopant with certain doping content could lead to a significant decrease in electrical resistivity and an increase in the optical band gap of ZnO [18]. When comparing the ionic radius of Ga and F to Zn and O, it is generally found that the ionic radius of Ga^{3+} (0.62 Å) is slightly lower than that of Zn^{2+} (0.74 Å) while F- has a very close ionic radius to

Corresponding Author E-mail: krisana_81@hotmail.com

O^{2-} (F^{-}: 1.31 Å and O^{2-}: 1.38 Å). According to this similarity in ionic radius and the higher charge of Ga^{3+} than Zn^{2+}, Ga would preferably replace the Zn host atom offering extra free electrons to the system, resulting in an enhancement in electrical conductivity and carrier mobility. Meanwhile, the higher electronegativity of F than O could lead to a higher distribution of electrons in the system. It is suggested that F may be a suitable anion doping candidate at O site, while Ga may be a suitable cation doping candidate at the Zn site in ZnO matrix. In the last few years, various ZnO nanostructures have been developed and applied in practical nanoelectronic and optoelectronic devices [19,20]. Diverse techniques such as chemical vapor deposition [21], metal-organic chemical vapor deposition (MOCVD) [22], electrodeposition [23], and hydrothermal method [24] have been employed for synthesizing low-dimensional ZnO nanostructures. The hydrothermal method has become one of the promising routes for growing nanomaterials because of its simplicity, ease of the equipped system, fastness, cost-effectiveness, and low operating temperature.

This work is conducted to investigate the role of Ga and F dopant on the relevant properties of ZnO nanostructures grown by hydrothermal process, especially their optical and electrical properties that can be scrutinized through photoluminescence spectroscopy.

2. Experimental details

The preparation of ZnO seeding layer, Ga-doped ZnO (GZO), and F-doped ZnO (FZO) nanorod-structures are described. First, the starting precursor for ZnO seed layer was prepared from zinc acetate dihydrate ($Zn(Ac)_2 \cdot 2H_2O$) and diethanolamine (DEA) dissolved in 100 mL absolute ethanol and stirred at 90 °C for 6 hr. The cleaned glass substrates were thoroughly dip-coated into the precursor solution and then dried on a hot-plate at 100 ºC for 15 min after each coating followed by annealing process in a furnace at 500 ºC for 2 hr. The precursor for the hydrothermal process was prepared by dissolving zinc nitrate hexahydrate ($Zn(NO_3)_2 \cdot 6H_2O$) and hexamethylenetetramine (HMTA)with DI water to achieve a 0.05 M solution. Ammonium fluoride (NH_4F) and gallium (III) nitrate hydrate (GaN_3O_9) was designated as F and Ga doping source, respectively. Each dopant precursor was added into Zn precursor to obtain a certain doping concentration of 5%. The substrates with ZnO seeding layer were sequentially immersed into the hydrothermal precursor then loaded into a Teflon autoclave for the hydrothermal synthesis operating at 90 ºC for 2 hr. After the operation time was reached, the obtained white solid product was separated from the solution by ultrasonic and was washed with DI water then dried in an oven at 100 ºC for 24 hr. The crystal structures and morphologies of all samples were characterized by XRD (Bruker D8 discover diffractometer) and FE-SEM (Hitachi S-4700), respectively. TG-DTA measurement of the from zinc acetate dihydrate precursor was carried out in air atmosphere with a heating rate of 2 ºC/min by Differential-Thermal Analyses (DTA, Perkin Elmer Pyris) for examining thermal behavior and decomposition of this precursor. The photoluminescence spectroscopy was conducted to investigate the related defects induced by dopant in the sample. Helium-Cadmium laser (λ = 325 nm) was used as an optical excitation source. Each sample was cooled down from room temperature (RT) to 25 K in a typical cryostat for temperature-dependent PL measurement. The luminescence spectra were collected by fiber optic spectrophotometer (Ocean Optics Inc. USB 4000).

3. Results and discussion

The thermal analyses by mean of differential temperature analysis (DTA) and thermogravimetric analysis (TG) were conducted to evaluate the thermal behavior of zinc acetate precursor. As noticed in the TG curve in Fig. 1, 60% weight loss of the precursor occurred at the temperature range of 200 °C – 250 °C that is associated with the loss of acetate groups. In addition, thermal decomposition at 258.29 °C in the DTG curve indicates the decomposition of residual organics before the formation of ZnO is initiated. An Insignificant thermal change was observed beyond this temperature, suggesting good thermal stability of the last product of starting precursor after decomposition.

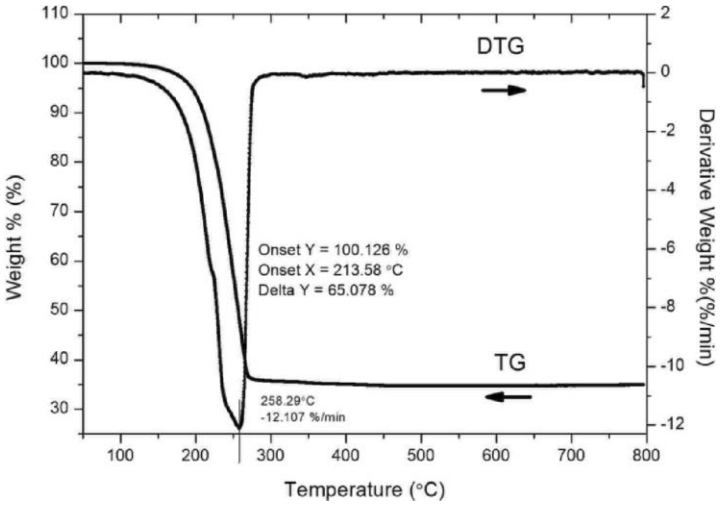

Fig. 1. TG-DTA data of zinc acetate sol-gel precursor.

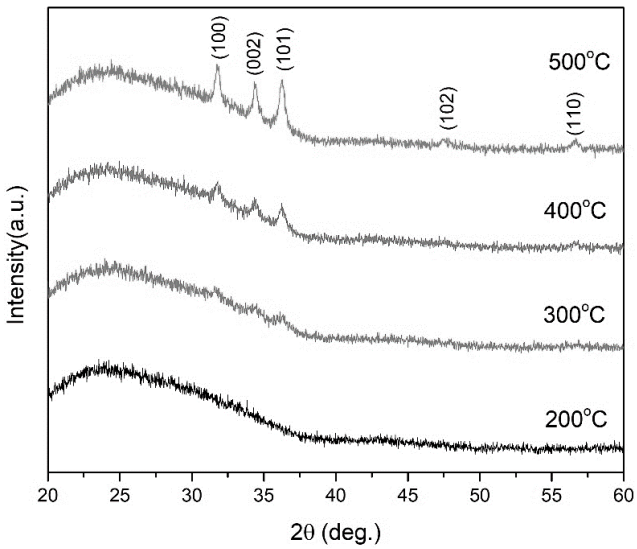

Fig. 2. XRD patterns of ZnO seed layers annealed at different temperatures of 200-500 ºC.

Fig. 2 shows XRD patterns of dip-coated ZnO seed layers annealed at different temperatures of 200 °C, 300 °C, 400 °C, and 500 °C. For the sample annealed at 200 °C, amorphous phase of the seed layer is observed since no characteristic diffracted peak is observed that is associated with the TG result. As the annealed temperature was elevated to 300 °C and 400 °C, the characteristic diffraction patterns of ZnO began to appear. This character indicates the change of the seed structure from amorphous to ZnO phase without preferential growth direction. The preferential orientation growth direction of ZnO sol-gel based film is highly influenced by the sol-gel concentration and grown particle-substrate interaction [25]. In this case, the amorphous behavior glass substrate could result in the random growth direction of ZnO particles without preferential orientation. The diffraction peaks became pronounced and the intensities increased significantly as annealing temperature was further increased at 500 °C owing to better ZnO crystallization. Three dominant peaks along (100), (002) and (101) planes are situated at 2θ = 31.8°, 34.5° and 36.2°, respectively. The orientation informed by XRD data of samples annealed at this temperature range indicates the polycrystalline nature of these seed layers. The crystal size can be calculated using Scherrer's relation expressed as

$$D = \frac{K\lambda}{\beta \cos\theta}. \quad (1)$$

Where D is the crystallite size of the sample, constant K (0.9) is the shape factor, λ is the X-ray wavelength of Cu K_α (0.154 nm), β is the full-width at half maximum (FWHM) of XRD peak, and θ is the Bragg angle. It is informed that the crystal size of the seed layer considerably increases from 12.4 nm to 26.2 nm as the annealing temperature increases from 400 ºC to 500 ºC, respectively. From this result, the annealing temperature of the seeding layer for further growth of ZnO, GZO, and FZO is determined at 500 ºC due to the good crystallinity of the seeding film.

Fig. 3 exhibits the cross-section SEM image of sol-gel derived ZnO seeding layer indicating that the layer is composed of uniform crystal grains with consistency in its thickness of about 165 nm.

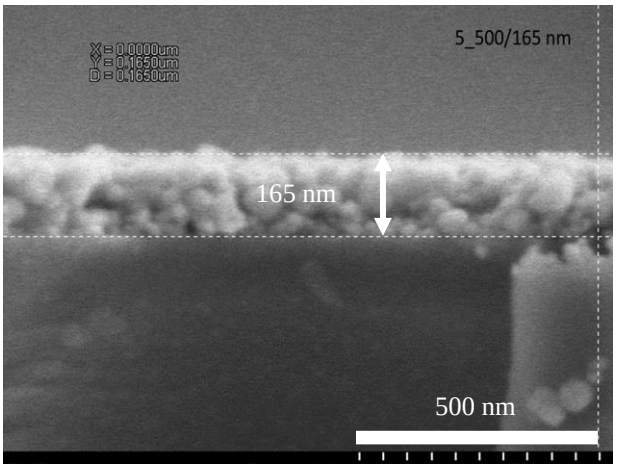

Fig. 3. Cross-section SEM image of ZnO seed layer annealed at 500 ºC.

Hydrothermally grown ZnO, GZO, and FZO nanorod-structured films were monitored by FE-SEM with corresponding images illustrated in Fig. 4 (a), (b), and (c), respectively. All samples exhibit hexagonal rod-like structures with a significant difference in shape, size, and alignment on the substrate. ZnO nanorods with an average rod size of ~100 nm are vertically aligned on the substrate. The bigger rod-like structures with random alignment on the substrate are observed in the GZO sample meanwhile FZO possesses smaller nanorod structures with sharper tip and average size less than 100 nm.

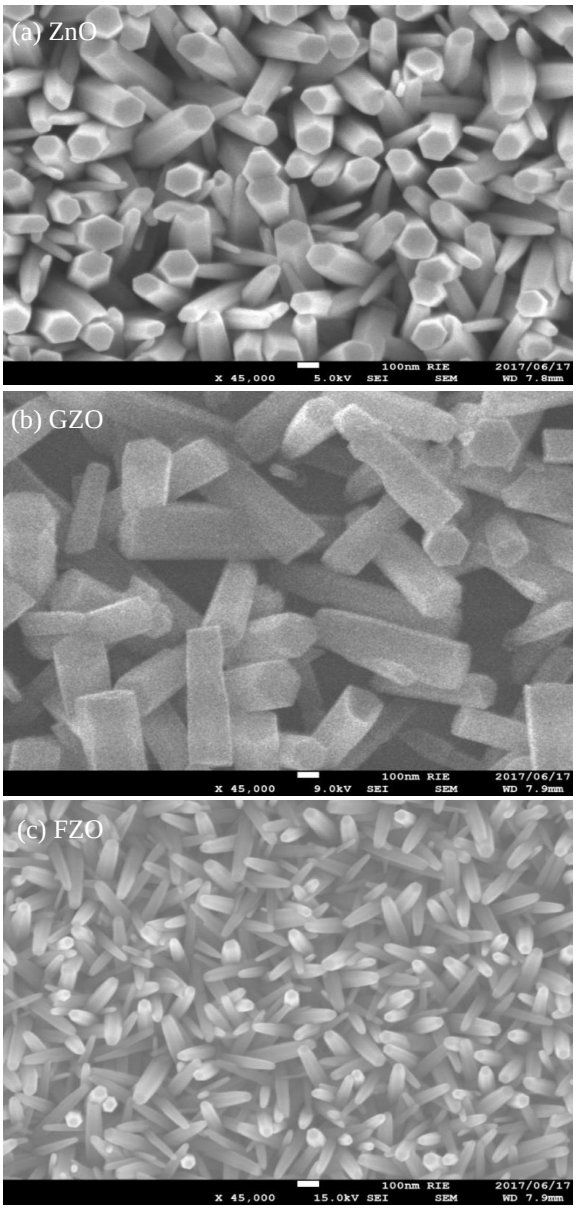

Fig. 4. FESEM images of (a) ZnO NRs, (b) GZO NRs, and (c) FZO NRs grown on ZnO seeding layer.

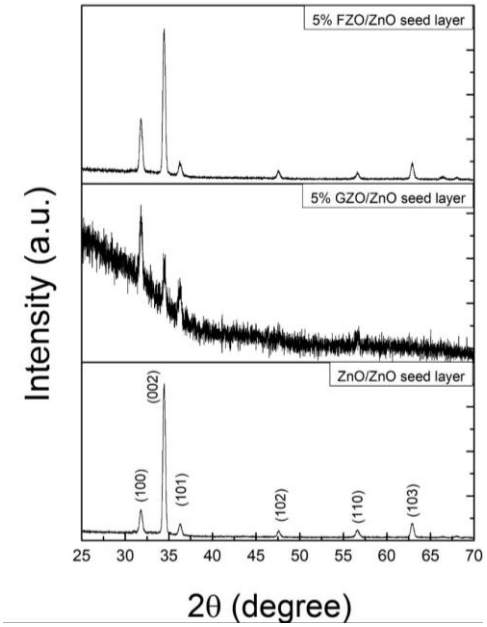

Fig. 5. XRD patterns of ZnO NRs (bottom) GZO NRs (middle) and FZO NRs (top) grown on ZnO seeding layer.

The corresponding XRD results of ZnO, GZO, and FZO nanostructures grown on ZnO seed layer are shown in Fig. 5. The clearly seen diffraction peaks positioned at 2θ = 31.77º, 34.42º, 36.25º, 47.54º and 56.60º in ZnO and FZO samples are assigned to (100), (002), (101), (102) and (110) orientation planes of ZnO with hexagonal wurtzite structure, respectively (JCPDS card No. 36-1451). For ZnO and FZO, the (002) orientation plane dominates other peaks, indicating the c-axis preferential growth direction of the grown rods. This result is well agreeable to the results observed by SEM images in Fig. 4 (top and bottom) However, the XRD patterns of GZO sample indicate hexagonal structure without any preferential direction of the grown structure that is in accordance with corresponding middle SEM image in Fig. 4.

Hydrothermally formed ZnO nanorods can be created via the following mechanisms. First, dissolved $Zn(NO_3)_2$ precursor is dissolved and provides zinc ions meanwhile ammonia molecules (NH_3) and hydroxide ions (HO^-) are provided by HMTA. NH_3 and HO^- rich-precursor could react with zinc ions to initially create $Zn(OH)_2$ via possible reaction in equation (2). This intermediate product can be further dissolved by reacting with superfluous HO^- ions to form $Zn(OH)_4^{2-}$ solution as expressed in equation (3). This $Zn(OH)_4^{2-}$ would undergo the dehydration process via equation (4) to initially form ZnO nuclei. These ZnO nuclei could be proceeded to form the rod-like nanostructures along with a preferred axis orientation depending upon growth conditions and dopants.

$$Zn^{2+} + 2OH^- \rightarrow Zn(OH)_2 \quad (2)$$

$$Zn(OH)_2 + 2OH^- \rightarrow Zn(OH)_4^{2-} \quad (3)$$

$$Zn(OH)_4^{2-} \rightarrow ZnO + H_2O + 2OH^- \quad (4)$$

It can be seen that ZnO and FZO have the hexagonal shape, suggesting ZnO nanorod grow along the (002) preferable direction with the fastest growth rate due to the lowest surface energy [26]. However, incorporated dopants may also greatly affect the growth rate of ZnO nanorod-structures along this direction by modifying its surface energies. It has been reported that Ga ions existing during ZnO low temperature (70 °C) hydrothermal growth can promote two-directional growth and suppress one-dimensional growth direction in (002) plane [27]. In this case, a higher process temperature of 90 °C could encourage electrostatic interaction between ions and the polar surface of ZnO that is highly sensitive to operating temperature. The preferential growth direction at this temperature would change to be along (002) plane [28] resulting in crystal growth in both lateral and vertical directions and consequently the appearance of short rod structure with large rod diameter as seen in Fig. 4(b). In the case of FZO sample, F doping anion with low doping content can be adsorbed on the specific polar surface and interacts with surface hydroxyl groups provided by HMTA and water to form hydrogen-bond ZnF(OH) species on the growth surface leading to passivation effect. At the first stage of rod growth. The existence of the species can partially inhibit (002) growth direction [26]. After an extended time, the deficiency of F anions results in the lack of ZnF(OH) in the system. At this stage, the preferable growth direction changes to (002) and consequently results in a sharp nanotip-rod structure of FZO sample.

Low-temperature photoluminescence spectra of ZnO, GZO, and FZO samples are illustrated in Fig. 6. It can be observed that all PL spectra obtained at low temperature (25 K) have similar features including three sharp UV emission bands (360-400 nm) and a broad yellow-orange visible emission band (500-700 nm). These three UV emission bands are generally ascribed to the near band edge emission of ZnO. The first peak with the shortest wavelength of ~368 nm is attributed to free exciton emission (FX) while the second dominant peak located at ~375 nm is typically associated with the emission of exciton of the bound shallow neutral donor (D^oX). Third peak situated at ~382 nm with broad is due to the donor to bound exciton emission [29-31]. The broad yellow-orange emission band could be deconvoluted to two Gaussian peaks located at 1.91 eV (λ~650 nm) and 2.15 eV (λ~580 nm) as depicted in Fig. 7. The yellow-orange emission is originated from the transition from the conduction band to deep level states of doubly ionized oxygen vacancies states (V_o^{+} and V_o^{++}) [32]. According to the NBE PL spectra of GZO and FZO, it can be observed that the intensity of D^oX and donor to bound exciton decreases significantly when comparing to ZnO sample, implying the suppression of these emissions by the dopants. When doping, the crystalline quality of ZnO could be decreased, reflecting the reduction of these NBE emission spectra. Moreover, as noticed in PL spectra of FZO, its PL intensity of yellow-orange emission is prominent comparing to the others. This feature suggests the existence of greater defect sites in the lattice of F-doped sample, implying the good incorporation of the F dopants that induce emission-related intrinsic defects of oxygen vacancies. The fundamental temperature-dependent luminescence of optical semiconductor material is considerably mandatory in basic science and technologically optoelectronic applications. Fig. 8 shows their photoluminescence spectra as a function of temperature ranging from 25 K to 285K. It is clearly seen that there is a significant red-shift of the major peak of UV-emission of all samples with increasing temperature. Two mechanisms are responsible for the temperature dependence of excitonic transitions of semiconductor materials including electron-phonon interaction and thermal expansion of the lattice. Furthermore, the broadening of this near band edge emission with increasing temperature is also noticed that due to the natural temperature-induced broadening mechanism in the semiconductor. Moreover, we have calculated the peak intensity ratios of visible broad emission to near-band-edge emission (I_{VIS}/I_{NBE}) of Ga and F dopant on PL emission at different temperatures (shown in Fig. 8(d)). It has been observed a much greater

enhancement ratio of visible broad emission (I_{VIS}) with the F dopant into ZnO structure, implying that the F dopant could highly induce oxygen vacancy defects in ZnO. The Ga substitution in the ZnO lattice may be responsible for the UV emission. The UV emission peak may probably come from donor zinc interstitial (Zn_i^O) to zinc interstitial with positive charges (Zn_i^+). On the other hand, F substitution in the ZnO lattice may be responsible for the yellow-orange emission. As the amount of oxygen vacancies is high, the yellow-orange emission peak may probably come from oxygen vacancy with a positive charge (V_o^+) to oxygen vacancy with two positive charges (V_o^{++}). Based on the PL results and I_{VIS}/I_{NBE} results, it can highly confirm the existence and the crucial roles of Ga and F dopant and substitution in the ZnO lattice.

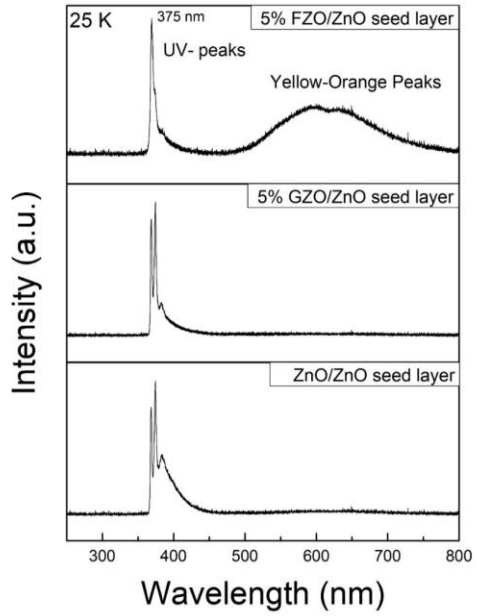

Fig. 6. Photoluminescence spectra of ZnO (bottom), GZO (middle), and FZO (top) nanostructures grown on ZnO seeding layer.

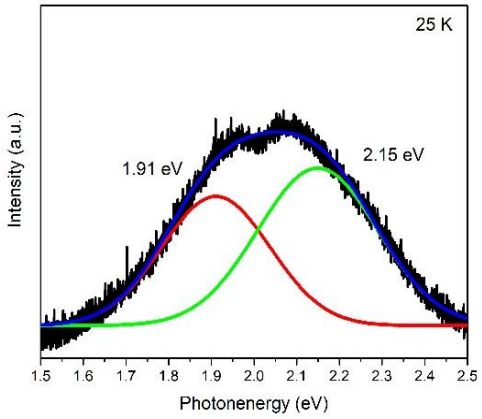

Fig. 7. Deconvolution of visible emission FZO nanostructure measured at 25 K.

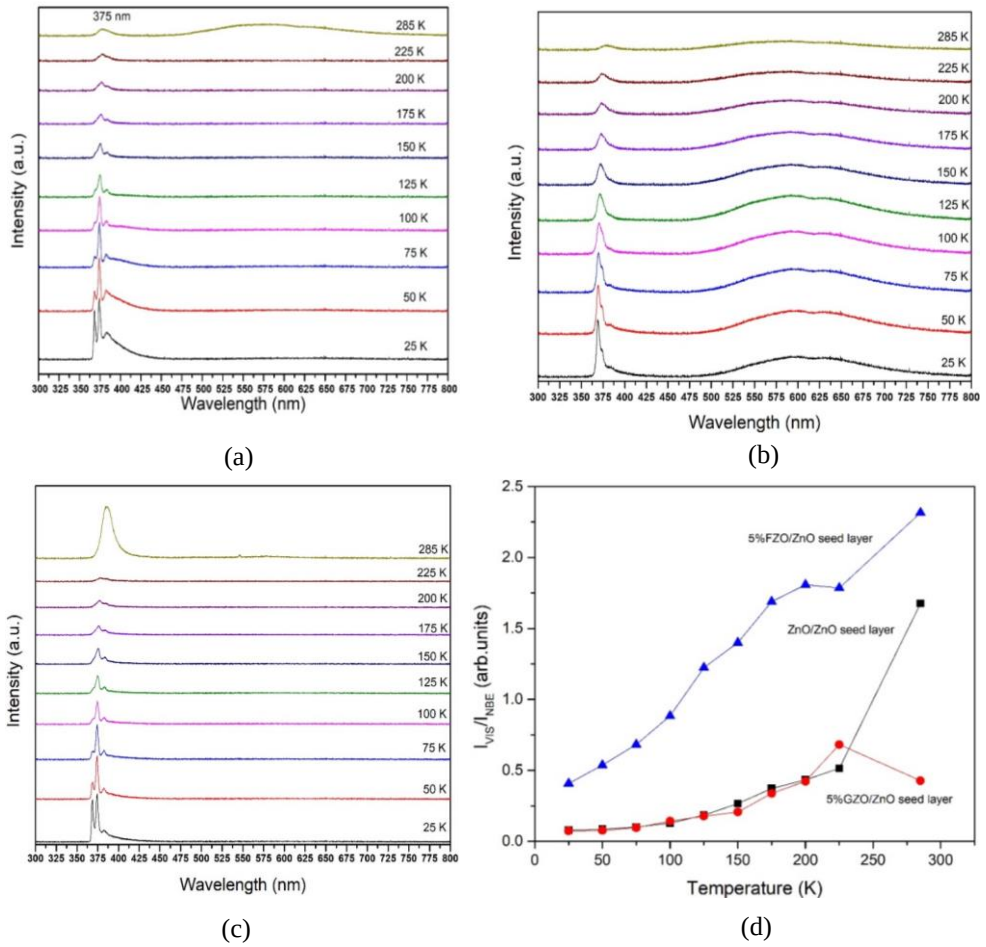

Fig. 8. Temperature-dependent photoluminescence spectra of (a) ZnO, (b) FZO, (c) GZO nanostructures grown on ZnO seeding layer, and (d) IVIS/INBE peak intensity ratio of all samples at different temperatures

4. Conclusion

ZnO nanorod-structures doped with Ga and F were grown by hydrothermal process onto ZnO sol-gel derived seeding film with a process temperature of 90 °C. Structural, morphological, and photoluminescence properties of the prepared samples were investigated. The annealing temperature for the seed layer was designated at 500 °C due to the good crystallinity of the film. ZnO and FZO nanorods are well aligned in the vertical direction while short GZO nanorods are randomly aligned on the substrate. The corresponding XRD and FE-SEM results suggest that different shapes of ZnO NRs, GZO NRs, and FZO NRs with different dopants can be obtained that are the key factors on the alternation in the morphology of the synthesized products. Moreover, the PL results can confirm the substitution of Ga and F dopant in the ZnO lattice.

Acknowledgement

Authors would like to thank Research Institute of Electronics, Shizuoka University for photoluminescence measurement. Krisana Chongsri would like to thank Rajabhat Rajanagarindra University for financial supports.

References

[1] Sandeep KM, Bhat Shreesha, SM Dharmaparakash. Structural, optical and LED characteristics of ZnO and Al doped ZnO thin films, J. Phys. Chem. Solids. 2017;104: 36-44.

[2] Patil VL, Vanalakar SA, Patil PS, Kim JH. Fabrication of nanostructured ZnO thin films based on NO_2 gas sensor via SILAR technique, Sensor Actuat. Sens. Actuators, B. 2017;239:1185-93.

[3] Khun K, Ibupoto ZH, Chey CO, Lu J, Nur O, Willander M. Comparative study of ZnO nanorods and thin films for chemical and biosensing applications and the development of ZnO nanorods based potentiometric strontium ion sensor. Appl. Surf. Sci. 2013;268: 37-43.

[4] Ferreira A, Silva JP, Rodrigues R, Martin N, Senentxu S, Méndez L, Vaz F. High performance piezoresistive response of nanostructured ZnO/Ag thin films for pressure sensing applications. Thin Solid Films. 2019;691:137587.

[5] Biswas C, Ma Z, Zhu X, Kawaharamura T, Wang KL. Atmospheric growth of hybrid ZnO thin films for inverted polymer solar cells. Sol. Energy Mater. Sol. Cells. 2016;157:1048-56.

[6] Guo ZL, Zhuang J, Ma Z, Xia HR, Wen QX, Luo XY, Wen X. Enhanced electron extraction using ZnO/ZnO-SnO_2 solid double-layer photoanode thin films for efficient dye sensitized solar cells. Thin Solid Films. 2019;684:1-8

[7] Shaikh SK, Inamdar SI, Ganbavle VV, Rajpure KY. Chemical bath deposited ZnO thin film based UV photoconductive detector. J. Alloys Compd. 2016;664:242-9.

[8] Zhang XL, Hui KS, Hui KN. High photo-responsivity ZnO UV detectors fabricated by RF reactive sputtering. Mater. Res. Bull. 2013;48(2):305-309.

[9] Soumya K, Selvam P, Potty SN. Study on the doping effect of spin coated Al and In doped and (Al/In) co-doped ZnO thin films for near-infrared plasmonic applications. Thin Solid Films. 2019;687:137482.

[10] Bharath SP, Bangera KV, Shivakumar GK. Enhanced gas sensing properties of indium doped ZnO thin films, Superlattices Microstruct. 2018;124:72-78.

[11] Horng R-H, Ou S-L, Huang C-Y, Ravadgar P, Wu C-I. Effects of Ga concentration and rapid thermal annealing on the structural, optoelectronic and photoluminescence properties of Ga-doped ZnO thin films. Thin Solid Films. 2016;605:30-36.

[12] Shkir M, Arif M, Ganesh V, Manthrammel MA, Singh A, Yahia IS, Maidur SR, Patil PS, Alfaify S. Investigation on structural, linear, nonlinear and optical limiting properties of sol-gel derived nanocrystalline Mg doped ZnO thin films for optoelectronic applications. J. Mol. Struct. 2018;1173:375-84.

[13] Salah N, Hameed A, Aslam M, Abdel-wahab MSh, Babkair SS, Bahabri FS. Flow controlled fabrication of N doped ZnO thin films and estimation of their performance for sunlight photocatalytic decontamination of water. Chem. Eng. J. 2016;291:115-127.

[14] Yuan H, Xu M. Influence of Na and F doping on microstructures, optical and magnetic properties of ZnO films synthesized by sol-gel method. Ceram. Int. 2018;44(13): 15531-34.

[15] Yamada Y, Inoue S, Kikuchi H, Funaki S. Resistivity reduction in Ga-doped ZnO films with a barrier layer that prevent Zn desorption. Thin Solid Films. 2018;657:50-54.

[16] Lung C, Toma M, Pop M, Marconi D, Pop A. Characterization of the structural and optical properties of ZnO thin films doped with Ga, Al and (Al+Ga). J. Alloys Compd. 2017;725:1238-1243.
[17] Li X, Hu Z, Liu J, Li D, Zhang X, Chen J, Fang J. Ga doped ZnO photonic crystals with enhanced photocatalytic activity and its reaction mechanism. Appl. Catal., B. 2016;195: 29-38.
[18] Rajkumar PV, Ravichandran K, Beneto M, Ravidhas C, Sakthivel B, Dineshbabu N. Enhancement of optical and electrical properties of SILAR deposited ZnO thin films through fluorine doping and vacuum annealing for photovoltaic applications. Mater. Sci. Semicond. Process. 2015;35:189-96.
[19] Kaps S, Bhowmick S, Gröttrup J, Hrkac V, Stauffer D, Guo H, Warren OL, Adam J, Kienle L, Minor AM, Adelung R, Mishra YK. Piezoresistive response of quasi-one-dimensional ZnO nanowires using an in-situ electromechanical device. ACS Omega. 2017;2:2985-93.
[20] Malik G, Mourya S, Jaiswal J, Chandra R. Effect of annealing parameters on optoelectronic properties of highly ordered ZnO thin films. Mater. Sci. Semicond. Process. 2019;100:200-13.
[21] Kumar RK, Husain M, Ansari ZA. Morphological variations and structural properties of ZnO nanostructures grown by rapid thermal CVD. J. Nanosci. Nanotechnol. 2011;11:6940-45.
[22] Chen H-G, Jian S-R, Li Z-W, Chen K-W, Li J-C. Epitaxial growth of self-arranged periodic ZnO nanostructures on sapphire substrates grown by MOCVD. J. Alloys Compd. 2010;504:S368-S371.
[23] Xue B, Liang Y, Donglai L, Eryong N, Congli S, Huanhuan F, jingjing X, Yong J, Zhifeng J, Xiaosong S. Electrodeposition from ZnO nano-rods to nano-sheets with only zinc nitrate electrolyte and its photoluminescence. Appl. Surf. Sci. 2011;257:10317-21.
[24] Yeo J, Hong S, Wanit M, Kang HW, Lee D, Grigoropoulos CP, Sung HJ, Ko SH. Rapid, one-Step, digital selective growth of ZnO nanowires on 3D structures using laser induced hydrothermal growth. Adv. Funct. Mater. 2013;23:3316-23.
[25] Cruz MRA, Como NH, Mejia I, Zarzosa GO, Castañón GAM, Lopez MAQ. Impact of the annealing atmosphere in the electrical and optical properties of ZnO thin films. J. Sol-gel Sci. Technol. 2016;79:184-9.
[26] Kang KM, Wang Y, Kim M, Park HH. Study on properties of Ga/F co-doped ZnO thin films prepared using atomic layer deposition. Thin Solid Films. 2018;660:913-9.
[27] Maeng J, Jo G, Choe M, Park W, Kwon MK, Park SJ, Lee T. Structural and photoluminescence characterization of ZnO nanowalls grown by metal organic chemical vapor deposition. Thin Solid Films. 2009;518:865-9.
[28] Guo M, Diao P, Cai S. Hydrothermal growth of well-aligned ZnO nanorod arrays: Dependence of morphology and alignment ordering upon preparing conditions. J. Solid State Chem. 2005;178:1864-73.
[29] Tsai Y Z, Wang N F, Tsai C L. Fluorine-doped ZnO transparent conducting thin films prepared by radio frequency magnetron sputtering. Thin Solid Films. 2010;518:4955-9.
[30] Alsultany F H, Hassan Z, Ahmed M N. Catalyst-free growth of ZnO nanowires on ITO seed layer/glass by thermal evaporation method: Effects of ITO seed layer laser annealing temperature. Superlattices Microstruct. 2016;92:68-79.
[31] Guo J, Zheng J, Song X, Sun K. Synthesis and conductive properties of Ga-doped ZnO nanosheets by the hydrothermal method. Mater. Lett. 2013;97:34-6.
[32] Zhu L, Li J, Ye Z, He H, Chen X, Zhao B. Photoluminescence of Ga-doped ZnO nanorods prepared by chemical vapor deposition. Opt. Mater. 2008;31:237-40.